UNIVERSITYOF BIRMINGHAM

Research at Birmingham

Modelling segregation effects of heterogeneous emissions on ozone levels in idealised urban street canyons: Using photochemical box models

Zhong, Jian; Cai, Xiaoming; Bloss, William

Link to publication on Research at Birmingham portal

Modelling segregation effects of heterogeneous emissions on ozone levels in idealised urban street canyons: using photochemical box models

Jian Zhong, Xiao-Ming Cai[*] and William James Bloss

School of Geography, Earth & Environmental Sciences, University of Birmingham, Edgbaston, Birmingham, B15 2TT, UK

[*]Corresponding author. Tel.: (0121) 4145533; Fax: (0121) 4145528.

Email address: x.cai@bham.ac.uk (X.-M. Cai).

Abstract

Air quality models include representations of pollutant emissions, which necessarily entail spatial averaging to reflect the model grid size; such averaging may result in significant uncertainties and/or systematic biases in the model output. This study investigates such uncertainties, considering ozone concentrations in idealised street canyons within the urban canopy. A photochemical model with grid-averaged emissions of street canyons is compared with a multiple-box model considering each canyon independently. The results reveal that the averaged, 'one-box' model may significantly underestimate true (independent canyon mean) ozone concentrations for typical urban areas, and that the performance of the averaged model is improved for more 'green' and/or less trafficked areas. Our findings also suggest that the trends of 2005-2020 in emissions, in isolation, reduce the error inherent in the averaged-emissions treatment. These new findings may be used to evaluate uncertainties in modelled urban ozone concentrations when grid-averaged emissions are adopted.

Capsule:

A grid-based urban air quality model, if adopting a grid-averaging scheme of emissions from segregated street canyons, may significantly underestimate the street-level ozone abundance.

Keywords: Segregation effect; urban street canyon; emission heterogeneity; photochemical box model; urban ozone concentrations.

Nomenclature

$C_{i,m}$: Concentration of ith species in Box m (m=0,1,2) (ppb);

$C_{bi,m}$: Background concentration of ith species for Box m (m=0,1,2) (ppb);

$C_{i,1+2}$: Averaged concentration of Boxes 1 and 2 of the ith species (ppb);

$E_{i,m}$: Emission rate of the ith species in Box m (m=0,1,2) (ppb s^{-1});

H_m: Height of the street canyon of Box m (m=0,1,2) (metre);

$I_{S(A+B)}$: Intensity of segregation between species A and B;

$k_{(A+B)}$: Second-order rate constant for species A and B in a well-mixed box;

$\langle k_{eff(A+B)} \rangle$: Effective second-order rate constant in the 'two-box' model;

RSL: Region Split Line;

t: Time (s);

$w_{t,m}$: Exchange velocity between street canyon and background for Box m (m=0,1,2) (m s^{-1});

$\Delta S_{i,m}$: Net chemical production rate of the ith species in Box m (m=0,1,2) (ppb s^{-1});

ε: Heterogeneity of emissions;

ϕ_i: Percentage of overestimation for the ith species by the 'one-box' model (%);

28

1 Introduction

30 Atmospheric chemical and physical processes are tightly coupled in air quality simulations
31 (Karamchandani et al., 2012). A general operating hypothesis of most urban air quality grid-
32 based models is that primary air pollutants emitted from vehicles, industry or other sources
33 are instantaneously well-mixed or distributed within the entire model grid-cell which contains
34 the emissions (Auger and Legras, 2007). The grid-averaged emission rates of primary air
35 pollutants are normally used as an input representing the mean gridded emissions (Denby et
36 al., 2011) in atmospheric chemical models and the concentration in the canopy layer is
37 modelled as one box representing the canopy layer for the entire grid cell. However, in reality
38 these surface emissions vary, and exhibit a high temporal and spatial heterogeneous
39 distribution at the sub-grid scale, referred to as surface sub-grid emission heterogeneity
40 (Galmarini et al., 2008). This leads to segregation effects due to incomplete mixing. In the
41 grid-averaging procedure, all sub-grid scale processes and features (Ching et al., 2006) are

42 lost and secondary pollutants (e.g. O_3) may therefore be systematically under- or over-
43 estimated.

44 Several model approaches have been suggested to account for the impacts of sub-grid
45 emission heterogeneity. Nested-grid or high-resolution modelling is a simple approach to
46 resolve sub-grid scale variablity. Examples of such approach can be seen from the
47 Community Multiscale Air Quality (CMAQ) model (Sokhi et al., 2006; Shrestha et al., 2009),
48 the Weather Research and Forecasting/Chemistry (WRF/Chem) model (Grell et al., 2005),
49 and the Comprehensive Air Quality Model with extensions (CAMx) (Shen et al., 2011). A
50 shortage of this approach is that it is only effective locally to a fixed area where the finer
51 resolution grid is located. In order to overcome the limitation, adaptive grid modelling
52 (Srivastava et al., 2000; Constantinescu et al., 2008; Garcia-Menendez et al., 2010) was
53 developed to allow dynamic change of the grid system during a simulation. Garcia-Menendez
54 and Odman (2011) discussed the details and reviewed the advances of the adaptive grid
55 modeling. Another approach to incorporate sub-grid emission heterogeneity is hydrid
56 modeling, which combines a regional grid-based model with a local Guassian dispersion
57 model (e.g. ADMS (Arciszewska and McClatchey, 2001) and AERMOD (Zou et al,2010)).
58 This approch has been extensively implemented, such as the CMAQ-ADMS model (Chemel
59 et al., 2011; Beevers et al., 2012; Stocker et al., 2012), the CMAQ-AERMOD model (Stein et
60 al., 2007; Isakov et al., 2009; Johnson et al., 2010) and the WRF-AERMOD model (Kesarkar
61 et al., 2007). A more promising approach is the plume-in-grid (PinG) modelling
62 (Karamchandani et al., 2002), which imbeds a non-steady-state plume model inside the grid.
63 Vijayaraghavan et al. (2006) implemented the plume-in-grid (PinG) modelling approach in
64 the CMAQ-APT model to reduce sub-grid scale variability in a simulation of central
65 California. They found that the sub-grid treatment can lead to up to 10 ppb less O_3 under the
66 condition of O_3 formation and up to 6 ppb more O_3 under other conditions, compared with a
67 base simulation without the PinG treatment. The approach offers a more realistic
68 representation of the elevated point emission sources and their atmospheric fate. Galmarini et
69 al. (2008) developed a Reynolds-average model to parameterize sub-grid emission
70 heterogeneity in the meso- and global scale. Their study built upon the assumption that
71 concentrations can be divided into a mean part, depending upon the average emissions, and a
72 fluctuation component which depends on the variabilty of emissions, respectively.
73 Alternatively, Cassiani et al. (2010) developed a stochastic fields method to address surface
74 sub-grid emission heterogeneity in a mesoscale dispersion model. The advantage of this

method is that the sub-grid scale emission variability is well-represented by the probability density functions. Some of the above approaches to address sub-grid scale errors are also reviewed and discussed in details by Touma et al. (2006) and Karamchandani et al. (2011). Currently, strategies to address sub-grid emission heterogeneity are mostly focussed upon large scale grid-based models. However, for the small scale, there is little research focusing on the effects of sub-grid emission heterogeneity.

Here, we extend consideration of emissions heterogeneity to the small scale, i.e. the canyon scale. The canopy layer is a major source for emissions into the overlying atmosphere / boundary layer and is normally within the lowest grid-cell of a grid-based model. From the canopy layer perspective, urban street canyons are typical sub-grid scale features seperated by rows of buildings. These emissions into the canyon layer may be pre-processed within urban street canyons before they enter to the entire grid-cell in the lowest part of the grid-based model (Fisher et al., 2006). Urban street canyons, where human exposure takes place, are the area of interest in this paper. The additional information between the grid-averaging implementation and the sub-grid calculation taking the emission heterogeneity into consideration may be of importance in terms of accurately calculating air pollutant abundance and their associated adverse health effects.

The aim of this study is to investigate segregation effects of heterogeneous emissions on O_3 levels in idealised urban street canyons, and to identify how segregation effects are influenced by the balance between chemistry and dynamics. The paper is structured as follows. In Section 2, the methodology based on photochemical box models is described in details, as well as the corresponding concept of intensity of segregation and the model scenarios. In the following sections, the results for prediction of ozone levels and the intensity of segregation are discussed.

2 Methodology

There are a large number of possible arrangements of street canyons in the urban canopy layer. In this study, we select two typical idealised urban street canyons as a representation. One large photochemical box model (hereafter referred to as the 'one-box' model) with averaged emissions of the two street canyons is used to represent the deterministic calculation based on the grid-average process; alternatively two small photochemical boxes (hereafter referred to as the 'two-box' model) are combined to represent two segregated street canyons with their own respective emissions. The photochemical box models (which assume that

107 chemical species inside each box are well-mixed) can be simply applied and computationally

108 inexpensive simulated. The model is written in FORTRAN77 language and run using

109 FACSIMILE 4 integrator (Curtis and Sweetenham, 1987). A reduced chemical scheme

110 (RCS), developed by Bright et al. (2013), is used as the chemical mechanism within the

111 photochemical box models. The detailed model configuration is described as follows.

112 2.1 Model Setup

113 Figure 1 illustrates the overview of the box model configuration. It is assumed that in a cell of

114 an urban air quality model, there are two street canyons with heterogeneous emissions

115 represented by Box 1 and Box 2 with the same volume of air as indicated in the right panel

116 (i.e. 'Two-box model') of Figure 1. There is no exchange between the two boxes, i.e. total

117 segregation is assumed; we only consider exchange between the within-canyon air and the

118 background air above the canopy layer. It is also assumed that the 'two-box' model

119 represents the reality and the mean concentration,

120 $$C_{i,1+2} = (C_{i,1} + C_{i,2})/2 \qquad (1)$$

121 represents the 'true' concentration of the ith species in the canopy layer corresponding to this

122 cell, with the concentrations in the 'one-box' model departing from this truth due to

123 segregation effects. If a simplified approach of one single box (Box 0 indicated in the left

124 panel of Figure 1) is adopted in which the volume of Box 0 is the sum of the volumes of Box

125 1 and Box 2 (indicated in the right panel of Figure 1) and $C_{i,0}$ is the modelled concentration

126 from the 'one-box' model (Box 0 in Figure 1), there would be an error for $C_{i,0}$ (either an

127 overestimation or an underestimation) in comparison with the 'true' mean concentration $C_{i,1+2}$

128 derived from the 'two-box' model (Box 1 and Box 2 in Figure 1). This error is expressed as

129 $$\Delta C_i = C_{i,0} - C_{i,1+2} \qquad (2)$$

130 We may also interpret ΔC_i as the concentration difference due to heterogeneity of emissions,

131 or the overestimated concentration by Box 0. For individual reactive species in the 'one-box'

132 model (Box 0), the mass transport can be described as the following equation (Liu and

133 Leung, 2008):

134 $$\frac{d}{dt}C_{i,0}(t) = E_{i,0} - \frac{w_{t,0}}{H_0}(C_{i,0} - C_{bi,0}) + \Delta S_{i,0} \qquad (3)$$

5

135   Where, $C_{i,0}$ (ppb) is the concentration of ith species by volume in Box 0, t (s) is the time, $E_{i,0}$

136   (ppb s^{-1}) is the emission rate of ith species by volume in Box 0, $w_{t,0}$ (m s^{-1}) is the exchange

137   velocity between the street canyon and background for Box 0, H_0 (m) is the height of the

138   street canyon of Box 0, $C_{bi,0}$ (ppb) is the background concentration of ith species of Box 0

139   and $\Delta S_{i,0}$ (ppb s^{-1}) is the net production rate of ith species due to chemical reactions in Box 0.

140   Similarly, the system of equations in the 'two-box' model (Box 1 and Box 2) can be

141   expressed as follows:

142
$$\frac{d}{dt}C_{i,1}(t) = E_{i,1} - \frac{w_{t,1}}{H_1}(C_{i,1} - C_{bi,1}) + \Delta S_{i,1} \tag{4}$$

143
$$\frac{d}{dt}C_{i,2}(t) = E_{i,2} - \frac{w_{t,2}}{H_2}(C_{i,2} - C_{bi,2}) + \Delta S_{i,2} \tag{5}$$

144   In Equations (4) and (5), all symbols are as those in Equation (3) but for Box 1 and Box 2,

145   respectively. In our model, we assume that $w_{t,0} = w_{t,1} = w_{t,2}$, $C_{bt,0} = C_{bt,1} = C_{bt,2}$,

146    $E_{i,1} = E_{i,0}(1+\varepsilon)$ and $E_{i,2} = E_{i,0}(1-\varepsilon)$, where ε is the heterogeneity of emissions for the two-

147   box model (e.g. $\varepsilon = 0$: homogeneous emissions for the two boxes; $\varepsilon = 1$: all emissions into

148   Box 1 and no emissions into Box 2). When the systems reach the steady state (or a quasi-

149   steady state) as $t \to t_s$, then $\frac{d}{dt}C_{i,m}(t) \to 0$ (m=0,1,2), and Equations (3)-(5) yield:

150
$$C_{i,0}(t_s) = \frac{H_0}{w_{t,0}}[E_{i,0} + \Delta S_{i,0}(t_s)] + C_{bi,0} \tag{6}$$

151
$$C_{i,1}(t_s) = \frac{H_1}{w_{t,1}}[E_{i,1} + \Delta S_{i,1}(t_s)] + C_{bi,1} \tag{7}$$

152
$$C_{i,2}(t_s) = \frac{H_2}{w_{t,2}}[E_{i,2} + \Delta S_{i,2}(t_s)] + C_{bi,2} \tag{8}$$

153
$$C_{i,1+2}(t_s) = [C_{i,1}(t_s) + C_{i,2}(t_s)]/2 \tag{9}$$

154   Thus the concentrations $C_{i,m}$ and the chemical production rate $\Delta S_{i,m}$, for m=0,1,2, are related

155   by above respective equations. The relationships are a function of the corresponding emission

156   rates and background conditions, respectively. It is noted that, from (2), (6)-(9), we have

157 $$\Delta C_i(t_s) = \frac{H_0}{w_{t,0}}[\Delta S_{i,0}(t_s) - \frac{\Delta S_{i,1}(t_s) + \Delta S_{i,2}(t_s)}{2}]$$ (10)

158 If the emission is a passive scalar (i.e. a species which does not undergo chemical reaction),

159 then the difference $\Delta C_i(t_s)$ is zero. For reactive species, the differences depend on the

160 heterogeneity of emissions and the nonlinear nature of photochemical reactions, together with

161 the exchange velocity caused by dynamic effects. Therefore the characteristics of $\Delta C_i(t_s)$

162 can be complex and will be examined in depth in the following sections.

163

164 Finally, we define the *percentage of overestimation* by the 'one-box' model (Box 0) for the ith

165 species as:

166 $$\phi_i(t) = \frac{\Delta C_i(t)}{C_{i,1+2}(t)} \times 100\%$$ (11)

167 $\phi_i(t)$ may also be interpreted as the overestimated concentration by the the 'one-box' model

168 relative to the 'true' concentration by the 'two-box' model. If $\phi_i(t) = 0\%$, it means that the

169 'one-box' model provides the true answer; if $\phi_i(t) = 10\%$ or -10%, it means that Box 0 over-

170 or under-estimates the concentration by 10%, respectively.

171 **2.2 Intensity of segregation**

172 In order to characterise the sub-grid scale variability due to incomplete mixing, a widely used

173 dimensionless number, the *intensity of segregation* (Krol et al., 2000) between two chemical

174 species A and B, $I_{S(A+B)}$, is introduced and defined as

175 $$I_{S(A+B)} = \frac{\langle A'B' \rangle}{\langle A \rangle \langle B \rangle}$$ (12)

176 where the angle brackets represent the volume average, the prime denotes the local deviation

177 from the volume-averaged concentration, and $A'B'$ stands for the covariance between A and

178 B. For any species A in the 'two-box' model of this study, $\langle A \rangle = \frac{1}{2}(A_1 + A_2)$ is A's mean

179 concentration of the two boxes, A_1 and A_2 are A's concentrations in Box 1 and Box 2,

180 respectively, $A_1' = A_1 - \langle A \rangle$, $A_2' = A_2 - \langle A \rangle$ and $\langle A'B' \rangle = \frac{1}{2}(A_1'B_1' + A_2'B_2')$. The intensity of

7

181   segregation between A and B is a proper measure of the effect of segregation on nonlinear

182   chemical processes (Hilst, 1998). For a second-order reaction $A+B \rightarrow C$ in a heterogeneously

183   system (i.e. the 'two-box' model in this study), the formation of C (Vinuesa and de Arellano,

184   2005) can be described as follows,

185    $$\frac{d\langle C \rangle}{dt} = \langle k_{eff(A+B)} \rangle \langle A \rangle \langle B \rangle \tag{13}$$

186   where $\langle k_{eff(A+B)} \rangle$ is the effective second-order rate constant for formation of C in the 'two-

187   box' model which can be represented by

188    $$\langle k_{eff(A+B)} \rangle = k_{(A+B)}(1 + I_{S(A+B)}) \tag{14}$$

189   where $k_{(A+B)}$ is the original rate constant of the reaction in the well-mixed 'one-box' model.

190   Such a constant is normally obtained from laboratory experiments in a well-mixed chamber.

191   If $I_{S(A+B)} = 0$, it means that species A and B can be regarded as well-mixed; If $I_{S(A+B)} > 0$ or

192    $I_{S(A+B)} < 0$, it implies that $\langle k_{eff(A+B)} \rangle$ in the 'two-box' model is larger or smaller than $k_{(A+B)}$ in

193   the 'one-box' model due to the effect of segregation.

194   **2.3   Model Scenarios**

195   **2.3.1 Initial and background conditions**

196   The initial conditions of the box models in this study were taken from those used in Bright et

197   al. (2013) which in turn were based upon atmospheric field data from the Tropospheric

198   Organic CHemistry (TORCH) experiment (Lee et al., 2006). The photochemical box model

199   is run without emissions for the first 30 minutes in order to spin up the model, which allows

200   concentrations of intermediate species to be calculated. Then the concentrations of all species

201   at 30 min are used as the background conditions in the boundary layer for exchange with the

202   inside canyon environment for all the simulations.

203   **2.3.2 Emissions and case settings**

204   Drawing upon the UK Road Vehicle Emission Factors (Boulter et al., 2009), emission rates

205   for NO_x, VOCs and CO of 620, 128 and 1356 g km^{-1} hr^{-1} were used respectively, which

206   represent an urban continuous road traffic of 1500 vehicles hr^{-1} with an average speed of 30

207 mph for the year of 2010 (Bright et al., 2013). The emission rates into a volume of urban

208 street canyons (18 m×18 m×1 m) are equivalent to E_{NOx}=0.28, E_{VOCs}=0.22 and E_{CO}=1.0 ppb

209 s^{-1} (here referred to a 'Typical Real-world Emission Scenario', TRES) for the NO_x, VOCs

210 and CO, respectively. This canyon geometry was used by Bright et al. (2013) for their large-

211 eddy simulations. In this study, E_{CO} is set as 1.0 ppb s^{-1} for all the scenarios, and the

212 representative E_{NOx} and E_{VOCs} are scaled by different factors between 0.1 and 2 in order to

213 characterize a wide range of real scenarios, i.e. E_{NOx} varies from 0.028 to 0.56 ppb s^{-1} in steps

214 of 0.028 ppb s^{-1}, while E_{VOCs} varies from 0.022 to 0.44 ppb s^{-1} in steps of 0.022 ppb s^{-1}. The

215 ratio of primary NO to NO_2 emission rate is 9:1, while the relative fractional VOCs emission

216 rates are 44% for C_2H_4, 19% for C_3H_6, 25% for HCHO and 12% for CH_3CHO (as mixing

217 ratio by volume) for all the scenarios.

218 In this study we focus on the effects of two parameters, ε (heterogeneity of emissions) and w_t

219 (exchange velocity), on ϕ_i and other characteristics. Table 1 gives an overview of the two

220 parameters for all cases. For each case, the corresponding one photochemical box model (i.e.

221 the 'one-box' model, Box 0) and two segregated photochemical box models (i.e. the 'two-

222 box' model, Box 1 and Box 2) were run. The heterogeneity of emissions (ε) is set at a value

223 of 0.5 and the exchange velocity (w_t) is set as 0.02 m s^{-1} in the base case, 'BASE'. The value

224 of ε=0.5 implies that the emissions into Box 1 (or Box 2) is 50% higher (or lower) than the

225 averaged emissions parameterized into Box 0. In reality, this is often the case; within an

226 Eulerian cell of an urban air quality model, some streets may have a much higher level of

227 traffic than others. The value of w_t=0.02 m s^{-1} is adopted based on the result from a large-

228 eddy simulation for a street canyon with a 18 m × 18 m cross-section under a neutral

229 condition if the reference wind speed is about 2 m s^{-1} (Cai, 2012).

230 In order to account for the segregation effect due to variations of ε and w_t, we examine in

231 detail the cases in which ε and w_t are perturbed by 40%, respectively. Case HE-L and HE-H

232 (see Table 1 for definitions) have been configured for 40% lower and higher ε, respectively,

233 than 0.5, while keeping the same w_t as that of Case BASE. To consider the effect of exchange

234 velocity (w_t), we set up the cases of EX-L and EX-H for 40% lower and higher w_t,

235 respectively, than 0.02 m s^{-1}, while keeping the same ε as that of Case BASE. The range of

236 values of w_t from 0.012 m s^{-1} to 0.028 m s^{-1} is justified based on previous findings that w_t

237 varies when the canyon aspect ratio (*H/W*, where *H* is the building height and *W* is the street

238 width) is altered from 1 to a higher or lower value (e.g. Chung and Liu, 2013) and that urban

239 surface heating may enhance w_t significantly (e.g. Cai, 2012).

3 Results and discussion

3.1 Overestimation of ozone levels

242 Figure 2 depicts $C_{O_3,1+2}$ (ppb), i.e. the 'true' concentration derived from the 'two-box' model,

243 for all cases listed in Table 1 as a function of E_{NOx} and E_{VOCs}, once the simulations had

244 reached a quasi-steady state (here defined as at $t = 4$ hr). The ranges of $C_{O_3,1+2}$ for all cases are

245 listed in Table 2, which reveals that the range of $C_{O_3,1+2}$ strongly depends on the variation of

246 w_t (indicated in Figure 2(d) and Figure 2(e)) rather than the variation of ε (indicated in Figure

247 2(b) and Figure 2(c)) and that the maximum range of $C_{O_3,1+2}$ is (5.62, 160.82) ppb for Case

248 EX-L with the lowest exchange velocity (0.12 m s^{-1}). In this study, the background O$_3$

249 concentration is approximately 43.61 ppb and by using a Region Split Line (RSL) we divide

250 the plot area into 2 regions, i.e. Region I (with the ratio of E_{VOCs} to E_{NOx} lower than the slope

251 of RSL) for which $C_{O_3,1+2}$ is lower than 43.61 ppb and Region II (with the ratio of E_{VOCs} to

252 E_{NOx} higher than the slope of RSL) for which $C_{O_3,1+2}$ is higher than 43.61 ppb. The RSL for

253 all cases is marked in Figure 2. Figure 2(f) indicates that the RSL for Cases BASE, HE-H and

254 HE-L exhibits the same slope with the $E_{VOCs}:E_{NOx}$ ratio (by volume) of 2.6, and the slopes of

255 the RSL are 1.9 for Cases EX-L and 3.4 for Cases EX-H (listed in Table 2). Therefore, we

256 may conclude that the slope of the RSL depends on w_t but not on ε, and that the higher w_t, the

257 higher the slope of the RSL. In Region I, the titration effect of O$_3$ by NO is dominant and

258 therefore leads to the net destruction of O$_3$ (i.e. lower than the background levels). However,

259 in Region II, OH oxidation processes are dominant and sufficient VOCs are present to

260 promote the conversion of NO to NO$_2$ by peroxy radicals, thereby causing net ozone

261 formation. It is therefore not surprising that $C_{O_3,1+2}$ is higher than its background level in

262 Region II. The TRES (i.e. $E_{NOx}=0.28$ ppb s^{-1}, $E_{VOCs}=0.22$ ppb s^{-1}) defined in Section 2.3.2 is

263 marked in the plots (triangle symbol); this emissions scenario, with the $E_{VOCs}:E_{NOx}$ ratio (by

264 volume) of 0.786, falls into Region I for all cases. This represents the typical situation in an

265 urban area, namely that the ozone concentration inside a street canyon is lower than that in

266 the overlying background atmosphere. It is noted in Figure 2(f) that the TRES is relatively

267 closer to the RSL for Case EX-L, in which the exchange velocity between the canyon and the

268 boundary layer aloft, w_t, is 40% lower than the base case. A low w_t might be caused by a

269 calm, stable meteorological condition or by a high canyon aspect ratio (i.e. large H/W). The

270 trajectory from 2005 to 2020 in Figure 2 represents the emission scenarios of these years,

271 which are derived from the UK fleet composition projections (NAEI, 2003) and the UK Road

272 Vehicle Emission Factors (Boulter et al., 2009) assuming constant traffic volume and speed

273 same as the 'TRES' for 2010. Figure 2 shows that the trajectory from 2005 to 2020 falls into

274 Region I and is approaching to the RSL with the reduction of VOCs and NO_x emissions due

275 to current and future control technologies, assuming constant activity (i.e. traffic) levels.

276

277 Figure 3 illustrates the transects of $C_{O_3,1+2}$ (ppb) through the emission scenarios in Figure

278 2(f). The rationale behind the choices is explained as follows. The dashed line, the dotted line

279 and the dot-dash line all pass through the point for the TRES, as marked in Figure 2(f). The

280 emission profile along this dashed line at the fixed E_{NOx} of 0.28 ppb s^{-1} (Figure 3(a))

281 represents a technology of targeting only E_{VOCs} from vehicles, or the roads with a varying

282 coverage of vegetation which may emit further VOCs into the urban canopy (Loughner et al.,

283 2012). The emission profile along this dotted line at the fixed E_{VOCs} of 0.22 ppb s^{-1} (Figure

284 3(b)) represents a technology of targeting only E_{NOx}. The emission profile along the dot-dash

285 line (Figure 3(c)) represents a technology of both E_{VOCs} and E_{NOx} ("TRES-2010") with the

286 proportional traffic-emitting rate of both VOCs and NO_x for the TRES. This dot-dashed line

287 may also represent control of the number of vehicles in streets or scenarios for different areas

288 (busier or less busy roads) with the same fleet composition as the TRES. The trajectory

289 (Figure 3(d)) indicates emission scenarios for the years 2005 to 2020 with the same traffic

290 volume and speed as the TRES. Figures 3(a) & 3(b) demonstrate that $C_{O_3,1+2}$ increases with

291 E_{VOCs} for the "Fixed E_{NOx}"scenario, but decreases with E_{NOx} for the "Fixed E_{VOCs}" scenario.

292 Figure 3(c) suggests that for less busier roads than the TRES, $C_{O_3,1+2}$ is higher, and vice

293 versa. Figure 3(d) shows that as control technologies are applied, $C_{O_3,1+2}$ increases. By 2020 it

294 will be very close to the background level, particularly for Case EX-L for which the canopy

295 layer is less ventilated. A higher ozone concentration also occurs to Case EX-L when E_{VOCs} is

296 very high for the "Fixed E_{NOx}" scenario (Figure 3(a)) or when E_{NOx} is very low for the "Fixed

297 E_{VOCs}" scenario (Figure 3(b)). The results show a nonlinear relationship between the O_3

298 concentration and E_{VOCs} and/or E_{NOx}, which is in line with many previous studies (e.g. Liu

299   and Leung, 2008). The TRES is indicated by a solid line in Figure 3(a)-(d) and $C_{O_3,1+2}$ for all

300   cases with the TRES are about 20 ppb with a small variation across those scenarios tested.

301   However, the analysis below demonstrates that these concentrations by the 'two-box' model

302   will be significantly underestimated by the 'one-box' model.

303

304   Figure 4 shows the values for ϕ_{O_3} (the percentage of overestimation for O_3 by the 'one-box'

305   model) for all cases listed in Table 1 at t=4 hr. It is interesting to notice that the RSL (defined

306   above) of each case splits the plot area into two regions, i.e. Region I where ϕ_{O_3} is negative

307   and Region II where ϕ_{O_3} is positive. In Region I, ϕ_{O_3} is negative, which means the modelled

308   O_3 concentration by the 'one-box' model is lower than the 'true' value by the 'two-box'

309   model (i.e. the 'one-box' model will underestimate O_3 levels). It is further shown that if only

310   ε is changed from 0.5 (Figure 4(a)) to 0.7 (Figure 4(c)) and to 0.3 (Figure 4(b)), respectively,

311   a rapid change in ϕ_{O_3} is found. The maximum underestimation could be up to -35.24 % for

312   Case HE-H (Figure 4(c)), and the minimum underestimation could be -6.12 % for Case HE-L

313   (Figure 4(b)). The larger ε is, the higher the maximum level of ϕ_{O_3} will be. It is also noted

314   that if only the exchange velocity (w_t) is changed from 0.020 m s^{-1} (Figure 4(a)) to 0.012 m s^{-1}

315   ^{1} (Figure 4(d)) and to 0.028 m s^{-1} (Figure 4(e)), respectively, there is a less significant change

316   in the maximum level of ϕ_{O_3} (listed in Table 2). However, there are noticeable shifts of the

317   RSL (discussed above) and the isopleths patterns associated with the variation of w_t. The

318   trajectory from 2005 to 2020 falls into the underestimation area (i.e. Region I), and is marked

319   in the plot for each case. In Region II for all the cases, the O_3 levels will be slightly over-

320   estimated up to 3.07 % obtained for Case HE-H (Table 2).

321

322   Figure 5 shows the transects of ϕ_{O_3} through the lines in Figure 4(f). For the TRES emission

323   scenario for the year of 2010 indicated by the solid line in Figure 5, underestimates of O_3

324   concentration by the 'one-box' model are -12.37% for Case BASE, -4.31% for Case HE-L, -

325   25.07% for Case HE-H, -8.90% for Case EX-L and -12.30% for Case EX-H, respectively,

326   suggesting that the effect of emission heterogeneity is more significant than the effect of

327   exchange velocity.

328

329　Figure 5(a) shows that as E_{VOCs} increases at the fixed E_{NOx} of 0.28 ppb s^{-1}, the modelled O_3

330　concentrations by the 'one-box' model are underestimated compared with the 'true' values,

331　indicated by the negative ϕ_{O_3}. The lower E_{VOCs} is, the larger the extent of underestimation

332　will be. Figure 5(a) also indicates that by keeping traffic-emission rate E_{NOx} unchanged, extra

333　E_{VOCs} (e.g. from vegetation or anthropogenic activities) will reduce ϕ_{O_3}, resulting in the

334　improved performance of the 'one-box' model. However, future reduction in vehicle-related

335　E_{VOCs}, anticipated to arise from renewal of the vehicle fleet and implementation of more

336　stringent emissions reduction technologies, will lead to an increase in the magnitude of ϕ_{O_3}.

337　This also suggests that the performance of the 'one-box' model for O_3 concentration might be

338　expected to be better for a more 'green' area, with biogenic VOC emissions, assuming such

339　emissions were not incorporated in the model scenario / conditions.

340

341　Figure 5(b) illustrates the results of ϕ_{O_3} along the dotted line of Figure 4(f), i.e. varying E_{NOx}

342　for a fixed E_{VOCs} corresponding to the TRES level of 0.22 ppb s^{-1}. The modelled O_3

343　concentrations by the 'one-box' model largely underestimate the 'true' values, indicated by

344　the negative ϕ_{O_3} (within Region I), with small positive values for ϕ_{O_3} only obtained at the

345　lowest E_{NOx} (within Region II). The magnitude of ϕ_{O_3} increases while E_{NOx} increases and the

346　maximum level of ϕ_{O_3} can be more than -30%. A large slope at the TRES for Case HE-H

347　suggests that reductions in vehicle NO$_x$ emissions anticipated to arise from renewal of the

348　vehicle fleet and implementation of more stringent emissions reduction technologies, will

349　lead to a reduction in the magnitude of ϕ_{O_3}, i.e. an improvement in model performance

350　overall.

351

352　Figure 5(c) shows the results of ϕ_{O_3} along the dot-dash line of Figure 4(f), i.e. varying E_{VOCs}

353　and E_{NOx} with the same emission ratio (i.e. 0.786) for the TRES (e.g. less or more trafficked

354　areas). It is noted that the performance of the 'one-box' model for a less trafficked

355　area/scenario (e.g. Birmingham) is better than that for a more trafficked area/scenario (e.g.

356　London). Figure 5(c) also shows that the effect of w_t on ϕ_{O_3} is relatively small for all cases.

357 However it is worth mentioning some secondary features that are counter intuititive, and thus

358 not easily interpreted. Firstly, there exists a threshold of (E_{NOx}, E_{VOCs}) below which, and

359 another threshold of (E_{NOx}, E_{VOCs}) above which, ϕ_{O_3} for Case EX-L and ϕ_{O_3} for Case EX-H are

360 on the opposing sides of ϕ_{O_3} for the base case; the first threshold of (E_{NOx}, E_{VOCs}) is about $6\times$

361 (0.028, 0.022) ppb s^{-1} and the second threshold of (E_{NOx}, E_{VOCs}) is about $10\times$(0.028, 0.022)

362 ppb s^{-1}. Between the two thresholds, the values of ϕ_{O_3} for both Case EX-L and Case EX-H are

363 larger than that for the case BASE. Secondly, according to intuition and linear reasoning, a

364 higher w_t (Case EX-H) implies a better ventilation of the two street canyons with the

365 background and in consequence a smaller difference between the two canyons; this effect

366 would be similar to a smaller ε (Case HE-L) that implies a smaller difference between the

367 two canyons. Therefore the points for Case EX-H (■) and Case HE-L (△) should appear on

368 the same side of Case BASE (O); likewise the points for Case EX-L (▲) and Case HE-H

369 (□) should appear on the same side of Case BASE (O). However, the results for O_3

370 concentration in Figure 3 do not always support the reasoning, neither do the results for ϕ_{O_3}

371 in Figure 5. These all indicate the complexity of the nonlinear chemical system and suggest

372 the necessity of in-depth analysis for specific scenarios.

373

374 Figure 5(d) shows the results of ϕ_{O_3} along the trajectory from the year of 2005 to 2020 as

375 indicated by Figure 4(f). It is noted that the level of extent of underestimation deceases with

376 year, which indicates that in the future the performance of the 'one-box' model will be better.

377 The underestimates of O_3 concentration by the 'one-box' model for the year 2020 are -3.91%

378 for Case BASE, -1.41% for Case HE-L, -7.60% for Case HE-H, -2.27% for Case EX-L and -

379 3.47% for Case EX-H, respectively.

380 **3.2　Intensity of segregation between O_3 and NO**

381 Figure 6 illustrates the results of $I_{S(O_3+NO)}$, the intensity of segregation between O3 and NO,

382 for all cases listed in Table 1 at the quasi-steady state (t=4 hr) as a function of E_{NOx} and E_{VOCs}.

383 It is interesting to notice that the RSL (defined above) of each case divides the plot area into

384 two regions, i.e. Region I where $I_{S(O_3+NO)}$ is negative and Region II where $I_{S(O_3+NO)}$ is

385 positive as indicated in Figure 6(a)-(e). The trajectory from the year of 2005 to 2020 falls into

386 the negative region (i.e. Region I), and is marked in the plot for each case. It can be shown

387 that the range of $I_{S(O_3+NO)}$ (listed in Table 2) increases rapidly while ε increases from 0.3 to

388 0.7, i.e. (-7.78 %, 1.79 %) for Case HE-L, (-21.29 %, 5.21 %) for Case BASE and (-40.98 %,

389 11.02%) for Case HE-H. The range of $I_{S(O_3+NO)}$ does not change significantly with the change

390 of the exchange velocity from 0.012 m s^{-1} to 0.028 m s^{-1}, i.e. (-21.12 %, 6.78 %) for Case

391 EX-L, (-21.29 %, 5.21 %) for Case BASE and (-21.18 %, 3.57) for Case EX-H. It is noted

392 that the plots of $I_{S(O_3+NO)}$ (Figure 6) are strongly correlated with those of ϕ_{O_3} (Figure 4). In

393 Region I for each case, the heterogeneity of emissions will lead to negative values of

394 $I_{S(O_3+NO)}$, which means that the effective rate constant of the titration reaction (NO + O$_3$ $\rightarrow$

395 NO$_2$ + O$_2$) to consume O$_3$, $\langle k_{eff(O_3+NO)} \rangle = k_{(O_3+NO)}(1 + I_{S(O_3+NO)})$, in the 'two-box' model is lower

396 than the original rate constant, $k_{(O_3+NO)}$, in the 'one-box' model. In other words, adopting the

397 classical rate constant $k_{(O_3+NO)}$ in the 'one-box' model results in too much titration. As a

398 result, the ozone level in the 'two-box' model (i.e. the 'true' value) is higher than the

399 modelled ozone level from the 'one-box' model, which agrees well with a negative value of

400 ϕ_{O_3}, i.e. the modelled ozone level from the 'one-box' model is underestimated. In Region II

401 for each case, a positive value of $I_{S(O_3+NO)}$ is observed, which indicates that $\langle k_{eff(O_3+NO)} \rangle$ is

402 larger than $k_{(O_3+NO)}$ and the 'true' value of O$_3$ is less than the modelled value of O$_3$ by the the

403 'one-box' model. Therefore, a positive value of ϕ_{O_3} is also observed in Region II, although

404 the maximum overestimation only reaches 3.07 % (Table 2) for those scenarios considered

405 here. Our findings also indicate that the slope of the RSL is determined by w_t (discussed

406 above), while the pattern and range of ϕ_{O_3} and $I_{S(O_3+NO)}$ in Region I and Region II depend

407 more closely on ε. It is also interesting to note that increasing ε will enhance the effect of

408 segregation and therefore promote sub-grid scale variability and potentially systematic error

409 in modelled O$_3$ abundance. It appears that the impact of change in ε and w_t on ϕ_{O_3} and

410 $I_{S(O_3+NO)}$ is nonlinear to E_{NOx} and E_{VOCs} due to the fact that O$_3$ is a secondary, rather than the

411 primary, pollutant.

412

413   Figure 7 shows the cross-sectional analyses, as indicated in Figure 6(f), of $I_{S(O_3+NO)}$ (%). For

414   the TRES emission scenario for the year of 2010 indicated by the solid line in Figure 7, the

415   values of $I_{S(O_3+NO)}$ are -15.47% for Case BASE, -5.38% for Case HE-L, -31.34% for Case

416   HE-H, -9.93% for Case EX-L and -17.37% for Case EX-H, respectively. It is noted that at the

417   fixed NO_x emission (Figure 7(a)), the magnitude of $I_{S(O_3+NO)}$ for all cases decreases (becomes

418   more negative) with reduced E_{VOCs}. However, at the fixed E_{VOCs} (Figure 7(b)), the value of

419      $I_{S(O_3+NO)}$ for each case decreases from positive to exclusively negative values with increased

420   E_{NOx} in Region II and then beomes increasingly negative as E_{NOx} continues to increase in

421   Region I. It is interesting that the smaller the values of ε or w_t (Figure 7(a) and Figure 7(b))

422   are, the smaller the magnitude of $I_{S(O_3+NO)}$ (compared with Case BASE) will be. It can be

423   seen from Figure 7(c) that $I_{S(O_3+NO)}$ becomes less negative for less trafficked area/scenario

424   and seems to be stable for the more polluted area/scenario. Figure 5(d) shows that the

425   magnitudes of $I_{S(O_3+NO)}$ decrease with year, suggesting that in the future the segregation

426   effect on ozone levels would be less signigicant. The comparison between the plots in Figure

427   7 with their equivalents in Figure 5 also indicates a strong relationship bewteen $I_{S(O_3+NO)}$ and

428   ϕ_{O_3}.

4   Conclusions

430   Segregation effects of heterogeneous emissions have been examined by considering the

431   surface sub-grid emission heterogeneity in two idealised urban street canyons within the

432   urban canopy layer and investigated how differing chemical effects (arising from the

433   heterogeneity of emissions) and dynamic effects (i.e. exchange velocity) influence the error

434   in O_3 if implementing the grid-averaging paramerization for heterogeneous emissions. This

435   study offers a better understanding of the paramerization of raw emissions for urban air

436   quality models by highlighting the importance of segregation effects of heterogeneous

437   emissions within the typical city-blocks (i.e. urban street canyons) and by providing a 2D

438   pattern of overestimation for O_3. The common situations in urban areas are found to fall into

439   Region I where the modelled O_3 concentration in street canyons (lower than that in the

440   overlying background atmosphere) by the 'one-box' model will be underestimated compared

441   with the 'true' value by the 'two-box' model. Our findings also indicate that the performance

442   of the 'one-box' model for O_3 concentration is better for a more 'green' area with extra VOCs

443 sources and for the less trafficked area/scenario. Future emission trends are expected to lead
444 to the error in the 'one-box' model approach falling. The error in ozone levels is strongly
445 linked to segregation effects of heterogeneous emissions and is balanced by both dynamics
446 and chemistry. This study is restricted to two boxes by considering only two typical street
447 canyons with emission hetergeneity, which are totally segregated, neither transported nor
448 mixed with each other. Future studies should take more photochemical boxes into
449 consideration and model more scenarios well represented by more street canyons. Our final
450 remark is that finding an appropriate real-world dataset to evaluate the box-averaged
451 concentrations of this study is challeging due to the fact that concentrations of chemical
452 species such as ozone are non-uniform inside a street canyon (Bright et al., 2013). Therefore
453 high spatial density observations of pollutant concentrations inside street canyons are needed
454 in support of a rigorous evaluation of the modelling approach. Recent development of low-
455 cost sensors (e.g. Mead et al. 2013) provides a potential for the task to be completed in the
456 future.

457

458

464

465

466

467

468   Table 1. Overview of the model scenarios

Case	Heterogeneity of emissions (ε)	Exchange velocity w_t (m.s^{-1})
BASE	0.5	0.02
HE-L	0.3	0.02
HE-H	0.7	0.02
EX-L	0.5	0.012
EX-H	0.5	0.028

Note: 'BASE' is the base case. 'HE' denotes the heterogeneity of emissions, while 'EX' means the exchange velocity. 'L' or 'H' represents a lower or higher value than the corresponding component in the base Case BASE.

469

470

471   Table 2. Overview of the range of values among emission scenarios for all cases

Case	$C_{O_3,1+2}$ (ppb) (min, max)	ϕ_{O_3} (%) (min, max)	$I_{S(O_3+NO)}$ (%) (min, max)	Slope of RSL (E_{VOCs}: E_{NOx})
BASE (ε=0.5, w_t=0.02 m s^{-1})	(7.56, 88.51)	(-17.35, 1.48)	(-21.29, 5.21)	2.6
HE-L (ε=0.3, w_t=0.02 m s^{-1})	(6.70, 89.16)	(-6.12, 0.52)	(-7.78, 1.79)	2.6
HE-H (ε=0.7, w_t=0.02 m s^{-1})	(9.69, 87.34)	(-35.24, 3.07)	(-40.98,11.02)	2.6
EX-L (ε=0.5, w_t=0.012 m s^{-1})	(5.62, 160.82)	(-17.31, 2.26)	(-21.12, 6.78)	1.9
EX-H (ε=0.5, w_t=0.028 m s^{-1})	(9.58, 68.13)	(-17.25, 0.82)	(-21.18, 3.57)	3.4

Note: 'BASE' is the base case. 'HE' denotes the heterogeneity of emissions, while 'EX' means the exchange velocity. 'L' or 'H' represents a lower or higher value than the corresponding component in the base Case BASE. $C_{O_3,1+2}$ denotes the true concentration of O$_3$ (ppb); ϕ_{O_3} means the *percentage of overestimation* for O$_3$ by the 'one-box' model (%); $I_{S(O_3+NO)}$ is the *intensity of segregation* between O$_3$ and NO (%); RSL represents the Region Split Line; E_{VOCs} and E_{NOx} are the emission rates of VOCs and NO$_x$, respectively (ppb s^{-1}).

472

473
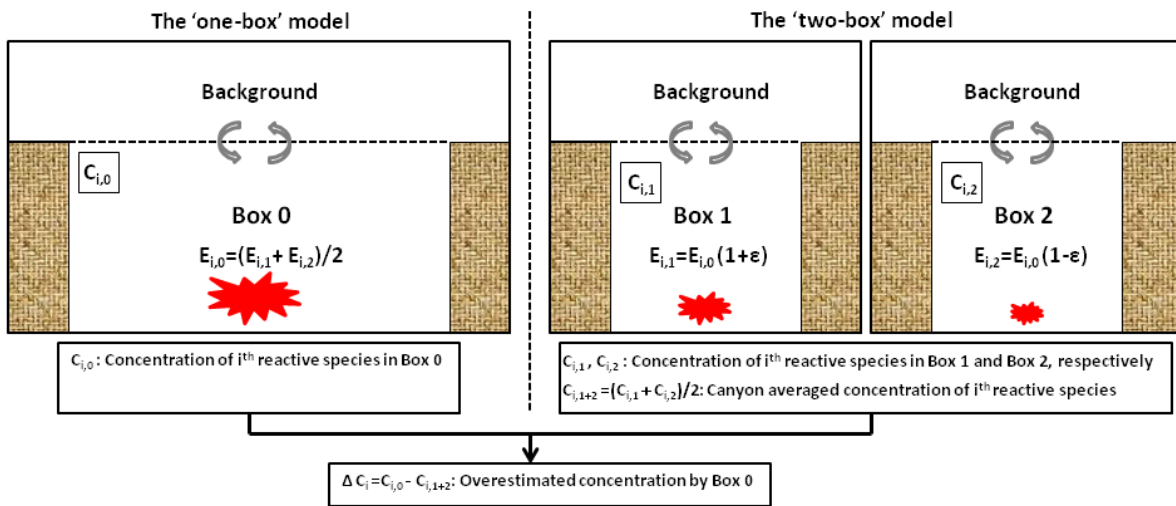
474

475   Figure 1. Overview of the model setup. $E_{i,m}$ means the emission rate of ith species in Box m (m=0,1,2) (ppb s^{-1});

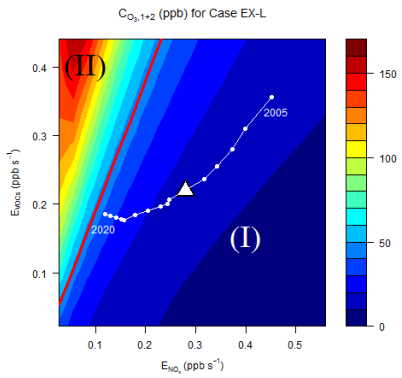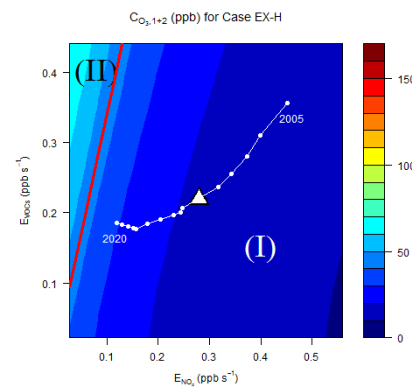476 ε is the heterogeneity of emissions.

(a) **(b)**

(c) **(d)**

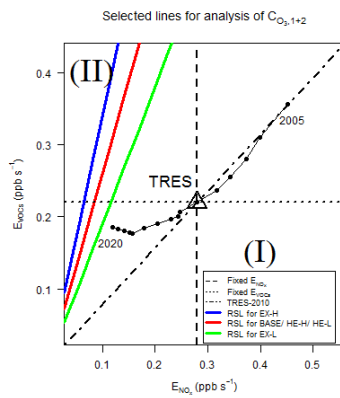**(e)** **(f)**
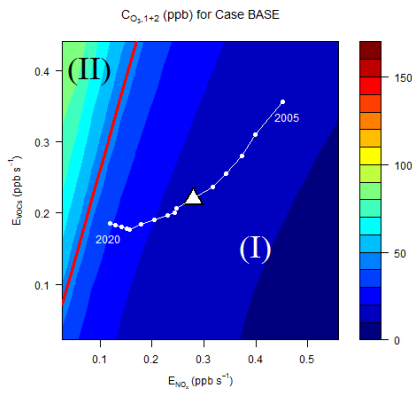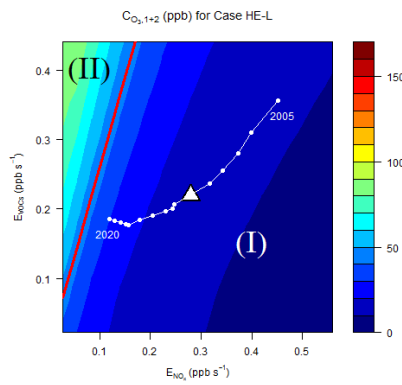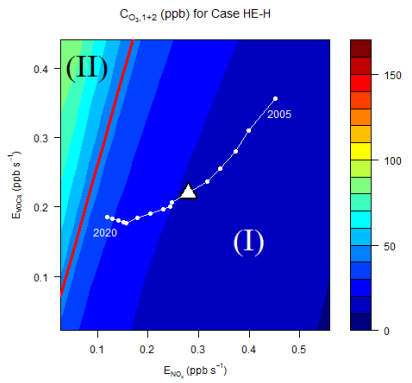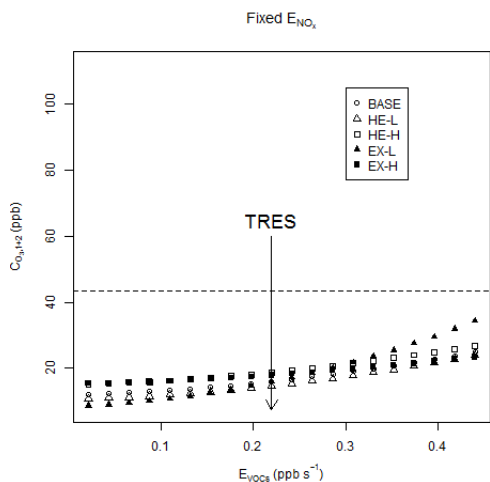
Figure 2. $C_{O_3,1+2}$ (ppb), the 'true' concentration of O_3 derived from the 'two-box' model, in the (a) Case BASE, (b) Case HE-L, (c) Case HE-H, (d) Case EX-L, (e) Case EX-H and (f) Selected lines for analysis. E_{VOCs} and E_{NOx} are the emission rates of VOCs and NO_x, respectively (ppb s^{-1}); RSL means Region Split Line; $\triangle$ represents the 'Typical Real-world Emission Scenario', TRES, for the year of 2010; The trajectory from 2005 to 2020 represents the emission scenarios for 2005 to 2020, assuming constant traffic volume and speed.

488

489

490   **(a)**   **(b)**

491

492   **(c)**   **(d)**

493
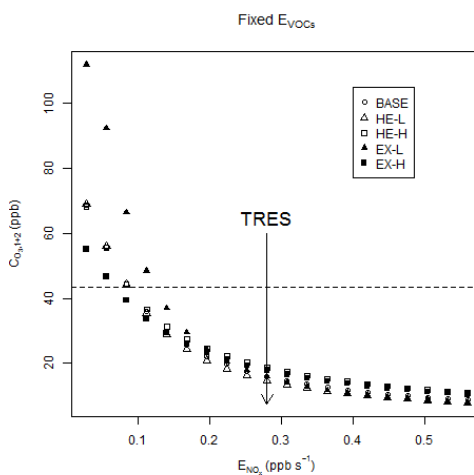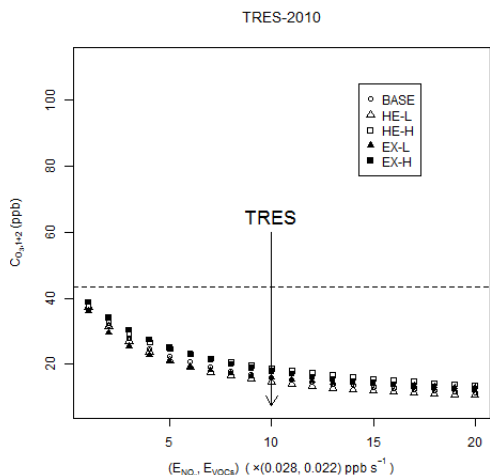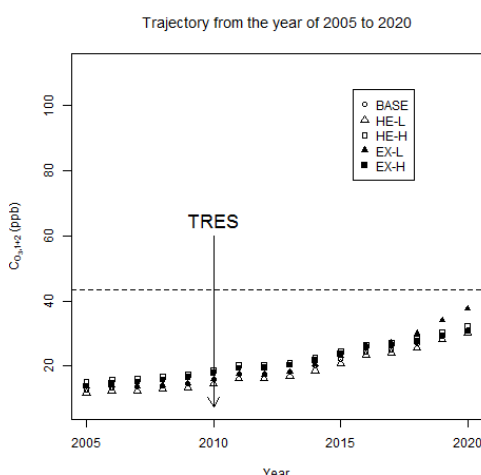
Figure 3. $C_{O_3,1+2}$ (ppb), the 'true' concentration of O_3 derived from the 'two-box' model, for (a) "Fixed E_{NOx}"
at a fixed NO_x emissions (0.28 ppb s^{-1}), (b) "Fixed E_{VOCs}" at a fixed VOCs emissions (0.22 ppb s^{-1}), (c) "TRES-
2010" varying the total traffic volume only and (d) "Trajectory from the year of 2005 to 2020" assuming
constant traffic volume and speed. E_{VOCs} and E_{NOx} are the emission rates of VOCs and NO_x, respectively (ppb s^{-1}); The
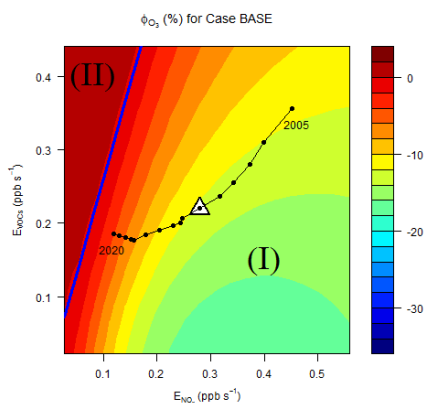dashed line indicates the background O_3 level of 43.61 ppb; The solid line indicates the 'Typical Real-world
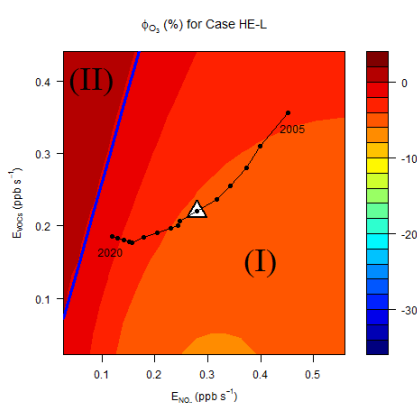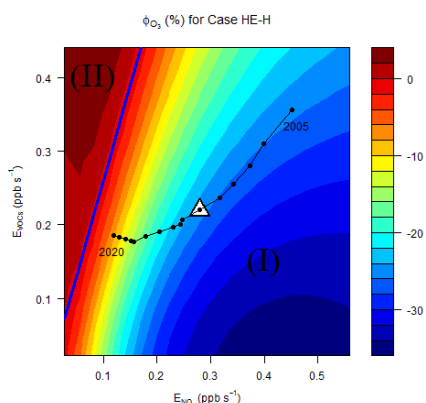Emission Scenario', TRES, for the year of 2010.

500

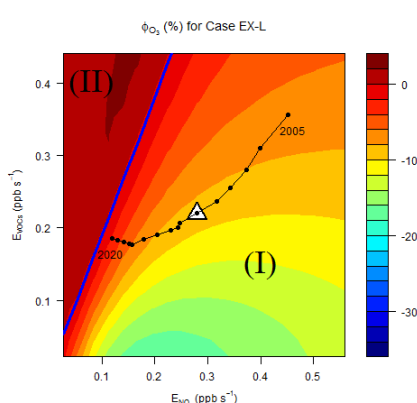501   **(a)**   **(b)**

502

503   **(c)**   **(d)**
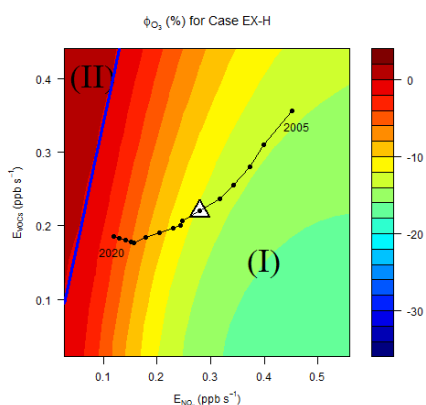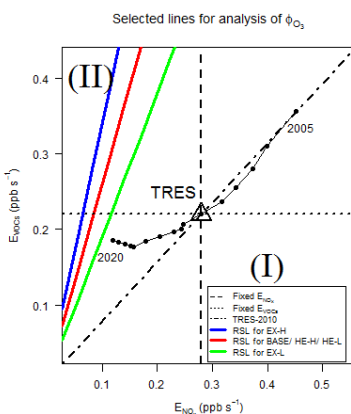

504

505   **(e)**   **(f)**

506

507   Figure 4. ϕ_{O_3} (%), the percentage of overestimation for O_3 by the 'one-box' model, in the (a) Case BASE, (b)

508   Case HE-L, (c) Case HE-H, (d) Case EX-L, (e) Case EX-H and (f) Selected lines for analysis. E_{VOCs} and E_{NOx} are

509   the emission rates of VOCs and NO_x, respectively (ppb s⁻¹); RSL means Region Split Line; △ represents the 'Typical

510   Real-world Emission Scenario', TRES, for the year of 2010; The trajectory from 2005 to 2020 means the

511   emission scenarios for 2005 to 2020, assuming constant traffic volume and speed.
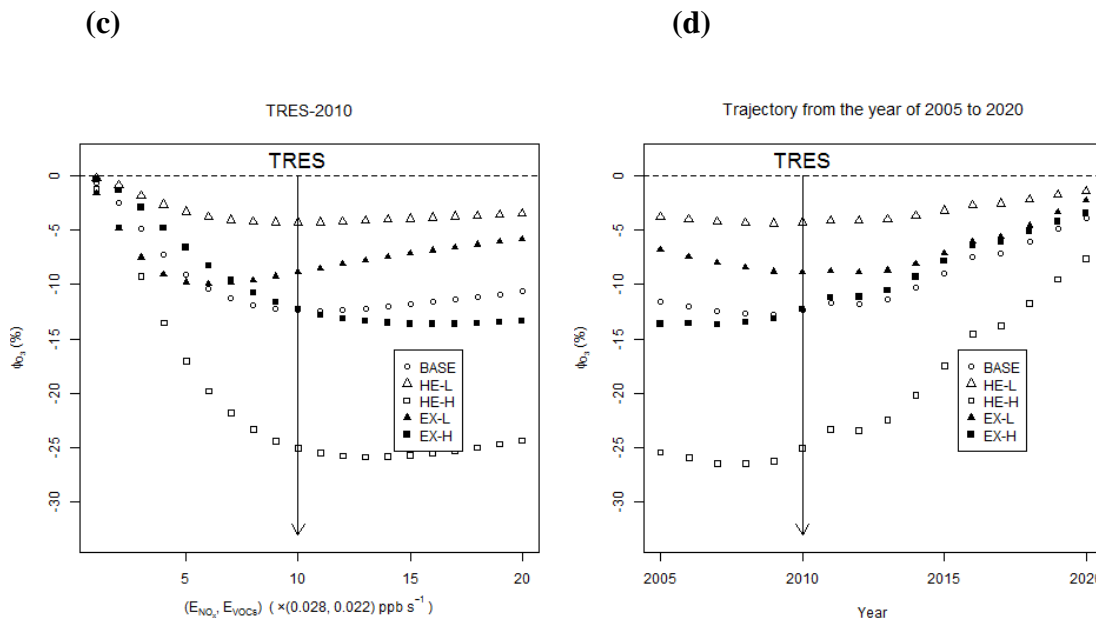
23

512

513 **(a)** **(b)**

514

515 **(c)** **(d)**

516
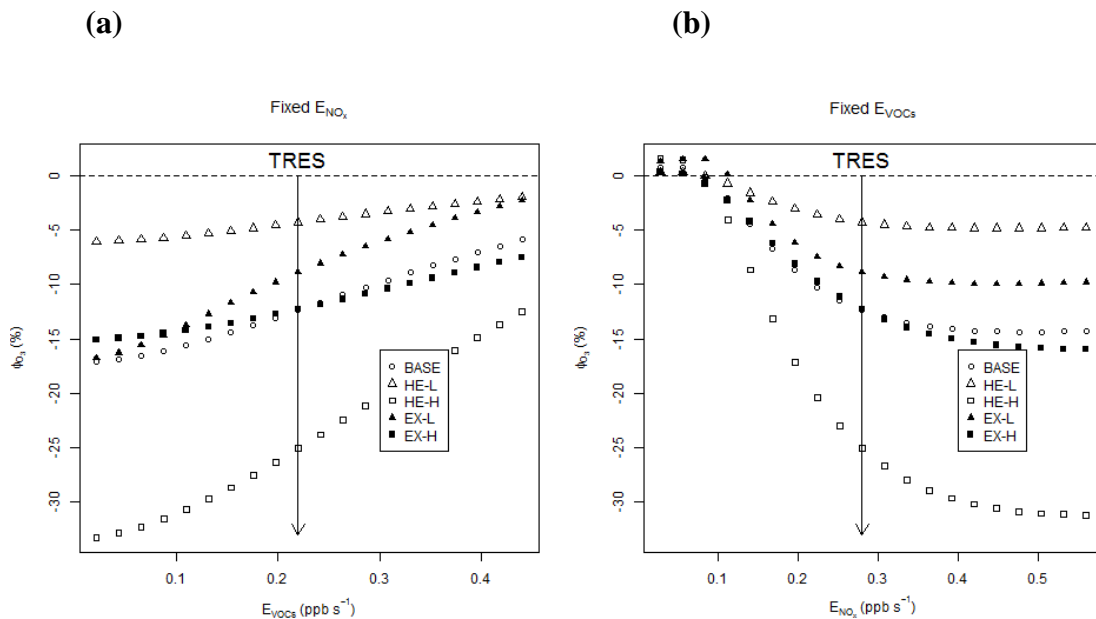
517 Figure 5. ϕ_{O_3} (%), the percentage of overestimation for O$_3$ by the 'one-box' model, for (a) "Fixed E_{NOx}" at a

518 fixed NO$_x$ emissions (0.28 ppb s^{-1}), (b) "Fixed E_{VOCs}" at a fixed VOCs emissions (0.22 ppb s^{-1}), (c) "TRES-

519 2010" varying the total traffic volume only and (d) "Trajectory from the year of 2005 to 2020" assuming
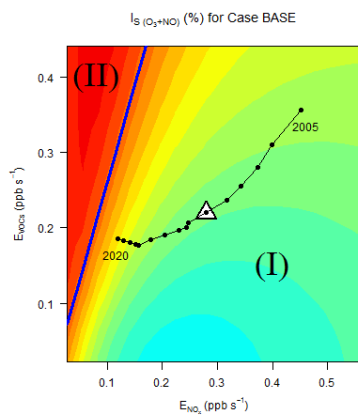
520 constant traffic volume and speed. E_{VOCs} and E_{NOx} are the emission rates of VOCs and NO$_x$, respectively (ppb s^{-1}); The

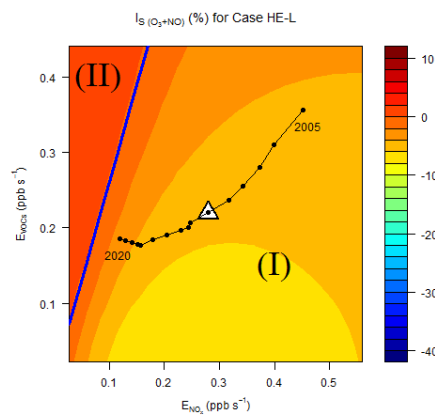521 solid line indicates the 'Typical Real-world Emission Scenario', TRES, for the year of 2010.
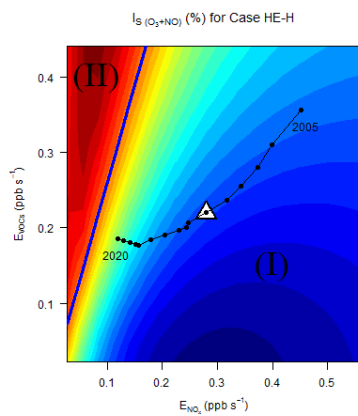
522

(a)   **(b)**

524

525   **(c)**   **(d)**

526

527   **(e)**   **(f)**

528
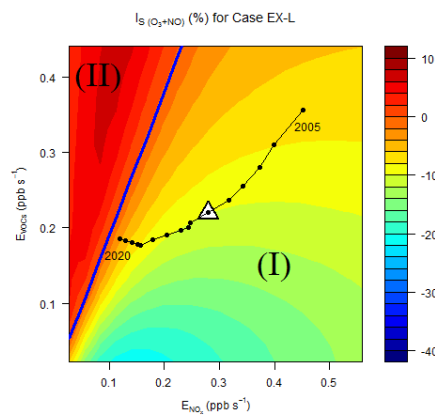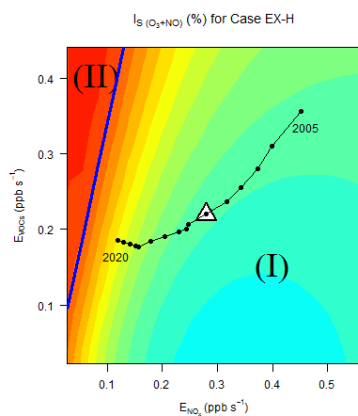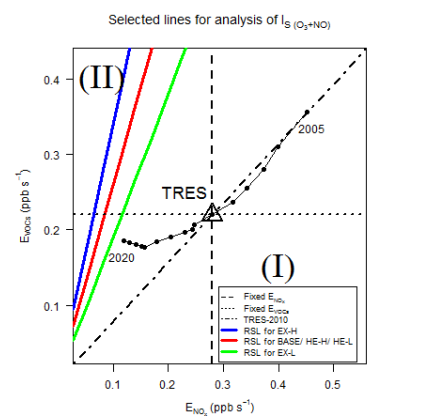
529 Figure 6. $I_{S(O_3+NO)}$ (%), the intensity of segregation between O$_3$ and NO, in the (a) Case BASE, (b) Case HE-

530 L, (c) Case HE-H, (d) Case EX-L, (e) Case EX-H and (f) Selected lines for analysis. E_{VOCs} and E_{NOx} are the

531 emission rates of VOCs and NO$_x$, respectively (ppb s^{-1}); RSL means Region Split Line; △ represents the 'Typical

Real-world Emission Scenario', TRES, for the year of 2010; The trajectory from 2005 to 2020 indicates the
emission scenarios for 2005 to 2020, assuming constant traffic volume and speed.

(a) **(b)**

(c) **(d)**
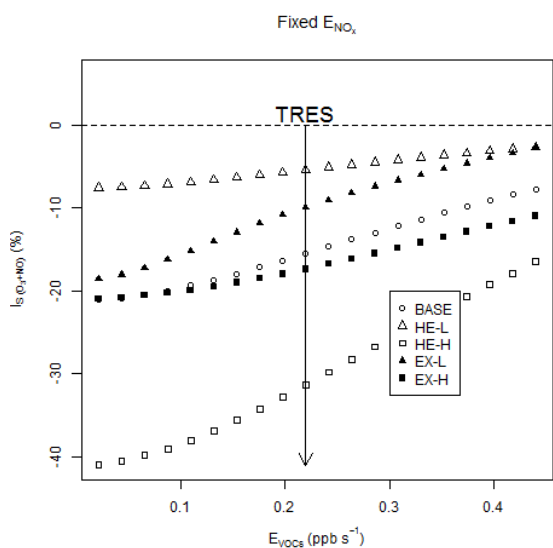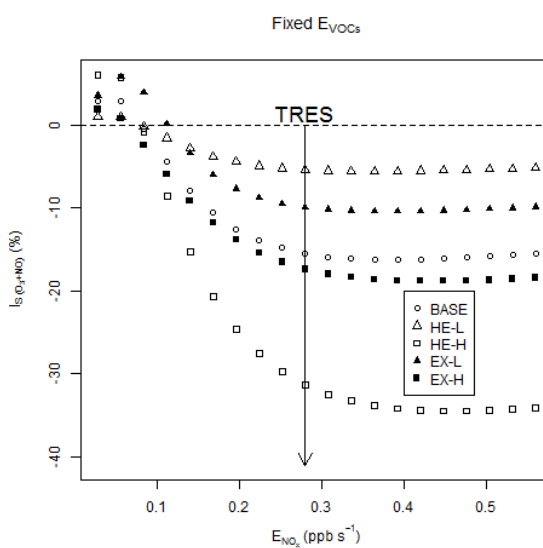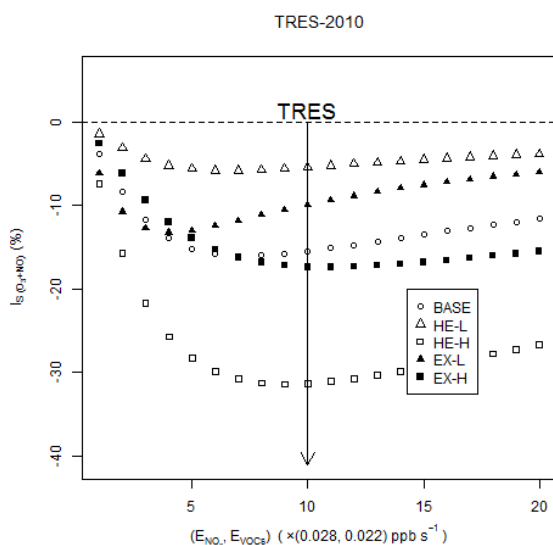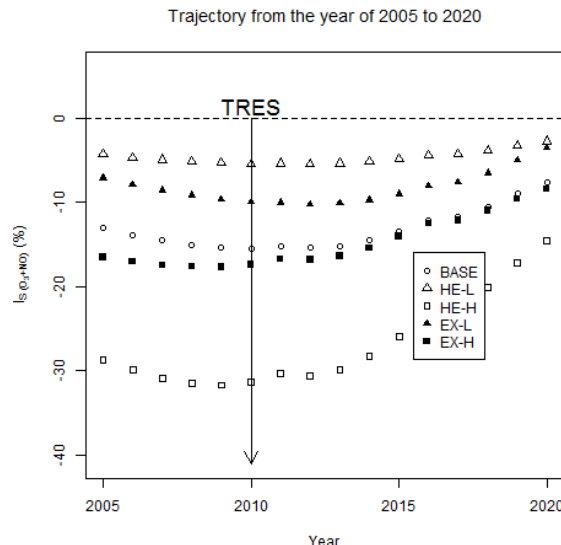
Figure 7. $I_{S(O_3+NO)}$ (%), the intensity of segregation between O_3 and NO, for (a) "Fixed E_{NOx}" at a fixed NO_x emissions (0.28 ppb s^{-1}), (b) "Fixed E_{VOCs}" at a fixed VOCs emissions (0.22 ppb s^{-1}), (c) "TRES-2010" varying the total traffic volume only and (d) "Trajectory from the year of 2005 to 2020" assuming constant traffic volume and speed. E_{VOCs} and E_{NOx} are the emission rates of VOCs and NO_x, respectively (ppb s^{-1}); The solid line indicates the 'Typical Real-world Emission Scenario', TRES, for the year of 2010.

References

544   **References**

545   Arciszewska, C. and McClatchey, J.: The importance of meteorological data for modelling air
546   pollution using ADMS-Urban. Meteorological Applications, 8, 345-350, 2001.

547   Auger, L. and Legras, B.: Chemical segregation by heterogeneous emissions. Atmospheric
548   Environment, 41, 2303-2318, 2007.

549   Beevers, S. D., Kitwiroon, N., Williams, M. L. and Carslaw, D. C.: One way coupling of
550   CMAQ and a road source dispersion model for fine scale air pollution predictions.
551   Atmospheric Environment, 59, 47-58, 2012.

552   Boulter, P. G., Barlow, T. J., Latham, S. and McCrae, I. S.: Emission Factors 2009: Report 1
553   - a review of methods for determining hot exhaust emission factors for road vehicles.
554   TRL: Wokingham, 2009.

555   Bright, V. B., Bloss, W. J. and Cai, X. M.: Urban street canyons: Coupling dynamics,
556   chemistry and within-canyon chemical processing of emissions. Atmospheric
557   Environment, 68, 127-142, 2013.

558   Cai, X.-M.: Effects of differential wall heating in street canyons on dispersion and ventilation
559   characteristics of a passive scalar. Atmospheric Environment, 51, 268-277, 2012.

560   Cassiani, M., Vinuesa, J. F., Galmarini, S. and Denby, B.: Stochastic fields method for sub-
561   grid scale emission heterogeneity in mesoscale atmospheric dispersion models.
562   Atmospheric Chemistry and Physics, 10, 267-277, 2010.

563   Chemel, C., Sokhi, R. S., Dore, A. J., Sutton, P., Vincent, K. J., Griffiths, S. J., Hayman, G.
564   D., Wright, R. D., Baggaley, M., Hallsworth, S., Prain, H. D. and Fisher, B. E. A.:
565   Predictions of UK Regulated Power Station Contributions to Regional Air Pollution
566   and Deposition: A Model Comparison Exercise. Journal of the Air & Waste
567   Management Association, 61, 1236-1245, 2011.

568   Ching, J., Herwehe, J. and Swall, J.: On joint deterministic grid modeling and sub-grid
569   variability conceptual framework for model evaluation. Atmospheric Environment,
570   40, 4935-4945, 2006.

571   Chung, T. N. H. and Liu, C.-H.: On the Mechanism of Air Pollutant Removal in Two-
572   Dimensional Idealized Street Canyons: A Large-Eddy Simulation Approach.
573   Boundary-Layer Meteorology, 148, 241-253, 2013.

574   Curtis, A. R. and Sweetenham, W. P.: FACSIMILE/CHECKMAT user's manual. UKAEA
575   Atomic Energy Research Establishment Computer Science and Systems Division,
576   1987.

577   Constantinescu, E. M., Sandu, A. and Carmichael, G. R.: Modeling atmospheric chemistry
578   and transport with dynamic adaptive resolution. Computational Geosciences, 12, 133-
579   151, 2008.

580   Denby, B., Cassiani, M., de Smet, P., de Leeuw, F. and Horalek, J.: Sub-grid variability and
581   its impact on European wide air quality exposure assessment. Atmospheric
582   Environment, 45, 4220-4229, 2011.

583   Fisher, B., Kukkonen, J., Piringer, M., Rotach, M. W. and Schatzmann, M.: Meteorology
584   applied to urban air pollution problems: concepts from COST 715. Atmospheric
585   Chemistry and Physics, 6, 555-564, 2006.

586 Galmarini, S., Vinuesa, J. F. and Martilli, A.: Modeling the impact of sub-grid scale emission
587   variability on upper-air concentration. Atmospheric Chemistry and Physics, 8, 141-
588   158, 2008.

589 Garcia-Menendez, F. and Odman, M. T.: Adaptive Grid Use in Air Quality Modeling.
590   Atmosphere, 2, 484-509, 2011.

591 Garcia-Menendez, F., Yano, A., Hu, Y. T. and Odman, M. T.: An adaptive grid version of
592   CMAQ for improving the resolution of plumes. Atmospheric Pollution Research, 1,
593   239-249, 2010.

594 Grell, G. A., Peckham, S. E., Schmitz, R., McKeen, S. A., Frost, G., Skamarock, W. C. and
595   Eder, B.: Fully coupled "online" chemistry within the WRF model. Atmospheric
596   Environment, 39, 6957-6975, 2005.

597 Hilst, G. R.: Segregation and chemical reaction rates in air quality models. Atmospheric
598   Environment, 32, 3891-3895, 1998.

599 Isakov, V., Touma, J. S., Burke, J., Lobdell, D. T., Palma, T., Rosenbaum, A. and Ozkaynak,
600   H.: Combining Regional- and Local-Scale Air Quality Models with Exposure Models
601   for Use in Environmental Health Studies. Journal of the Air & Waste Management
602   Association, 59, 461-472, 2009.

603 Johnson, M., Isakov, V., Touma, J. S., Mukerjee, S. and Ozkaynak, H.: Evaluation of land-
604   use regression models used to predict air quality concentrations in an urban area.
605   Atmospheric Environment, 44, 3660-3668, 2010.

606 Karamchandani, P., Seigneur, C., Vijayaraghavan, K. and Wu, S. Y.: Development and
607   application of a state-of-the-science plume-in-grid model. Journal of Geophysical
608   Research-Atmospheres, 107, 2002.

609 Karamchandani, P., Vijayaraghavan, K. and Yarwood, G.: Sub-Grid Scale Plume Modeling.
610   Atmosphere, 2, 389-406, 2011.

611 Karamchandani, P., Zhang, Y. and Chen, S. Y.: Development and initial application of a sub-
612   grid scale plume treatment in a state-of-the-art online Multi-scale Air Quality and
613   Weather Prediction Model. Atmospheric Environment, 63, 125-134, 2012.

614 Kesarkar, A. P., Dalvi, M., Kaginalkar, A. and Ojha, A.: Coupling of the Weather Research
615   and Forecasting Model with AERMOD for pollutant dispersion modeling. A case
616   study for PM10 dispersion over Pune, India. Atmospheric Environment, 41, 1976-
617   1988, 2007.

618 Krol, M. C., Molemaker, M. J. and de Arellano, J. V. G.: Effects of turbulence and
619   heterogeneous emissions on photochemically active species in the convective
620   boundary layer. Journal of Geophysical Research-Atmospheres, 105, 6871-6884,
621   2000.

622 Lee, J. D., Lewis, A. C., Monks, P. S., Jacob, M., Hamilton, J. F., Hopkins, J. R., Watson, N.
623   M., Saxton, J. E., Ennis, C., Carpenter, L. J., Carslaw, N., Fleming, Z., Bandy, B. J.,
624   Oram, D. E., Penkett, S. A., Slemr, J., Norton, E., Rickard, A. R., Whalley, L. K.,
625   Heard, D. E., Bloss, W. J., Gravestock, T., Smith, S. C., Stanton, J., Pilling, M. J. and
626   Jenkin, M. E.: Ozone photochemistry and elevated isoprene during the UK heatwave
627   of August 2003. Atmospheric Environment, 40, 7598-7613, 2006.

628 Liu, C.-H. and Leung, D. Y. C.: Numerical study on the ozone formation inside street
629   canyons using a chemistry box model. Journal of Environmental Sciences-China, 20,
630   832-837, 2008.

631 Loughner, C. P., Allen, D. J., Zhang, D.-L., Pickering, K. E., Dickerson, R. R. and Landry,
632   L.: Roles of Urban Tree Canopy and Buildings in Urban Heat Island Effects:
633   Parameterization and Preliminary Results. Journal of Applied Meteorology and
634   Climatology, 51, 1775-1793, 2012.

635 Mead, M.I., Popoola, O.A.M., Stewart, G.B., Landshoff, P., Calleja, M., Hayes, M., Baldovi,
636   J.J., McLeod, M.W., Hodgson, T.F., Dicks, J., Lewis, A., Cohen, J., Baron, R.,
637   Saffell, J.R., Jones, R.L.,. The use of electrochemical sensors for monitoring urban air
638   quality in low-cost, high-density networks. Atmospheric Environment 70, 186-203,
639   2013.

640 NAEI: UK fleet composition projections. URL: http://naei.defra.gov.uk/data/ef-transport,
641   2003.

642 Shen, J., Wang, X. S., Li, J. F., Li, Y. P. and Zhang, Y. H.: Evaluation and intercomparison
643   of ozone simulations by Models-3/CMAQ and CAMx over the Pearl River Delta.
644   Science China-Chemistry, 54, 1789-1800, 2011.

645 Shrestha, K. L., Kondo, A., Kaga, A. and Inoue, Y.: High-resolution modeling and evaluation
646   of ozone air quality of Osaka using MM5-CMAQ system. Journal of Environmental
647   Sciences-China, 21, 782-789, 2009.

648 Sokhi, R. S., San Jose, R., Kitwiroon, N., Fragkou, E., Perez, J. L. and Middleton, D. R.:
649   Prediction of ozone levels in London using the MM5-CMAQ modelling system.
650   Environmental Modelling & Software, 21, 566-576, 2006.

651 Srivastava, R. K., McRae, D. S. and Odman, M. T.: An adaptive grid algorithm for air-quality
652   modeling. Journal of Computational Physics, 165, 437-472, 2000.

653 Stein, A. F., Isakov, V., Godowitch, J. and Draxler, R. R.: A hybrid modeling approach to
654   resolve pollutant concentrations in an urban area. Atmospheric Environment, 41,
655   9410-9426, 2007.

656 Stocker, J., Hood, C., Carruthers, D. and McHugh, C.: ADMS-Urban: developments in
657   modelling dispersion from the city scale to the local scale. International Journal of
658   Environment and Pollution, 50, 308-316, 2012.

659 Touma, J. S., Isakov, V., Ching, J. and Seigneur, C.: Air quality modeling of hazardous
660   pollutants: Current status and future directions. Journal of the Air & Waste
661   Management Association, 56, 547-558, 2006.

662 Vijayaraghavan, K., Karamchandani, P. and Seigneur, C.: Plume-in-grid modeling of summer
663   air pollution in Central California. Atmospheric Environment, 40, 5097-5109, 2006.

664 Vinuesa, J. F. and de Arellano, J. V. G.: Introducing effective reaction rates to account for the
665   inefficient mixing of the convective boundary layer. Atmospheric Environment, 39,
666   445-461, 2005.

667 Zou, B., Zhan, F. B., Wilson, J. G. and Zeng, Y. N.: Performance of AERMOD at different
668   time scales. Simulation Modelling Practice and Theory, 18, 612-623, 2010.